High-Spatial Resolution Resistivity Mapping of Large-Area YBCO Films by a Near-Field Millimeter-Wave Microscope

Michael Golosovsky, Alexander Galkin, and Dan Davidov

Abstract— **We demonstrate a new millimeter-wave technique for the resistivity mapping of large-area conducting films, namely, a near-field resistivity microscope. The microscope is based on the idea that electromagnetic waves are transmitted through a narrow resonant slit with high efficiency. By scanning this slit at fixed height above an inhomogeneous conducting surface and measuring the intensity and phase of the reflected wave, the resistivity of this surface may be determined with a 10–100 μm spatial resolution using 80-GHz radiation. Using this technique, we map normal-sate resistivity of 1 in $\times$ 1 in YBCO films at ambient temperature. In some films we find inhomogeneities of the normal-state sheet resistance of the order of 10%–20%.**

I. Introduction

Microwave applications of high-T_c superconductors require large-area uniform films. Therefore, it is very important to control the uniformity of their electrical properties, such as resistivity. There are several methods of resistivity mapping, each of them having a specific area of applications. For example, the tunneling [1], capacitance [1], and electron [2] microscopics provide nanometer resolution, however they have a very small field of view $\sim$1 μm, and hence are not suitable for large-area samples inspection. On the contrary, the four-point [3], confocal resonator [4], and mutual inductance techniques [5] are able to map large-area samples, but their spatial resolution is not high—$\sim$1 mm. In order to bridge the gap between 1 μm and 1 mm spatial resolutions, the methods of the near-field microscopy [6] may be applied. This microscopy employs a probe of a subwavelength size and an object that is mounted in the near-field of the probe. The spatial resolution of the near-field microscopy is determined by the probe size rather than by the wavelength. The probe may be a small circular aperture in the conducting screen [6], a miniature coaxial tip [7], [8], an open waveguide or a dielectrically filled parallel-plate antenna [9], a microstrip resonator [10], a small SQUID [11]. A general problem in near-field rf-microscopy is the compromise between the size of the probe and its transmittance. To achieve high spatial resolution, one must employ very small probes. The price paid usually is that the transmittance of small probes rapidly drops with decreasing size. Nevertheless, there are few near-field probes that have high transmittance in the certain bandwidth (for example, a coaxial cable). In the present work we propose a new near-field probe for the resistivity mapping, namely, *a resonant slit*. We demonstrate that this probe combines high spatial resolution with high transmittance.

II. Theory of Operation

The most important part of our device is an aperture in the form of a narrow resonant slit. Consider a thin metal diaphragm mounted across a rectangular waveguide. A window in the form of a rectangular slit is cut in this diaphragm parallel to the wide side. For the TE-mode propagation, this window is transparent at a certain wavelength λ

Manuscript received October 20, 1995; revised February 12, 1996. This work was supported by the Klatchky foundation, the European community, and the Bergman foundation.

The authors are with the Racah Institute of Physics, Hebrew University of Jerusalem, Jerusalem 91904, Israel.

Publisher Item Identifier S 0018-9480(96)04787-4.

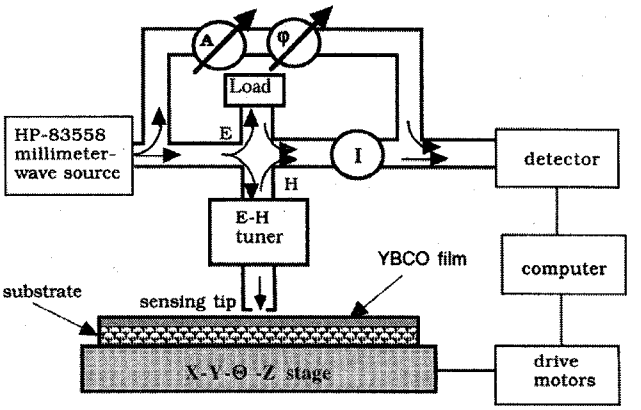

Fig. 1. A scanning millimeter-wave near-field microscope. It is based on the E-band millimeter-wave bridge and a resonant slit as a sensing probe. The sample is mounted in the near-field of the probe. Reflection of the millimeter-wave depends on the resistivity of the small sample spot under the probe. By raster scanning the sample under the probe and measuring the imbalance signal of the bridge, the resistivity map is yielded. The sensing probe is a narrow slit cut in the end-plate of the waveguide. The length of the slit is approximately equal to $\lambda/2$ (where λ is the wavelength in the free space), while the width may be exceedingly small.

[12], which is found by solving

$$\frac{a}{b}\sqrt{1-\left(\frac{\lambda}{2a}\right)^2}=\frac{a'}{b'}\sqrt{1-\left(\frac{\lambda}{2a'}\right)^2}. \tag{1}$$

Here λ is the free-space wavelength, a and b are the wide and narrow dimensions of the waveguide, and a' and b' are the wide and narrow dimensions of the slit. It is important to note that (1) has solution even for arbitrarily narrow slit. Namely, if $b' \to 0$ then $\lambda \to 2a'$. A further insight into the resonant slit operation may be achieved using an analogy between a rectangular waveguide terminated by a rectangular slit window and a junction of two rectangular waveguides with different narrow sides [13]. The reflection from such a junction is determined by the waveguide impedance

$$Z_s=\frac{Z_0\pi b'}{2a'\sqrt{1-\left(\frac{\lambda}{2a'}\right)^2}} \tag{2}$$

where Z_0 is the free-space impedance ($Z_0 = 377\ \Omega$). We apply this expression to the slit, treating it as a section of a rectangular waveguide, and observe that for given a' and arbitrarily small b' there is always a certain wavelength $\lambda \approx 2a'$ at which $Z \approx Z_0$. Therefore, we expect that even a very narrow slit may be narrow-band matched to free space.

If the resonant slit antenna is put very close to a conducting surface, so that this surface is in the near-field zone, then the microwave is reflected mostly from the region under the slit. Since reflection from conducting surfaces is determined by the resistivity, by measuring the amplitude and phase of the reflected wave while raster scanning the surface, it is possible to map the microwave resistivity. For thick conductive layers (much thicker than the skin-depth) this procedure yields surface impedance, while for thin layers it yields sheet resistance. To determine microwave resistivity in this latter case, it is necessary to measure layer thickness independently.

Provided the distance between the slit and the surface is smaller than the narrow dimension of the slit, the spatial resolution in the direction perpendicular to the slit is determined by the slit's width b'

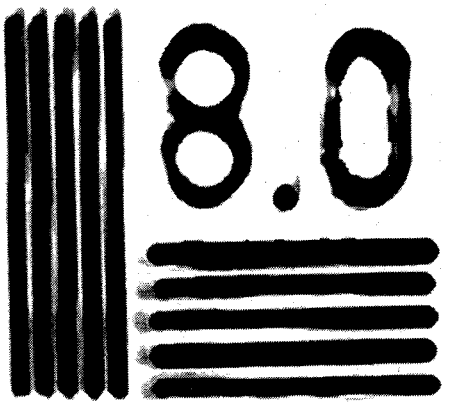

Fig. 2. A gray scale image of a section of the NIST 1963a test target (Cr coating on a glass substrate, linewidth is 63 μm). $f = 79.6$ GHz ($\lambda = 3.8$ mm), incident power is 0.5 mW. The reference arm of the bridge is tuned to compensate reflection from the glass substrate. The spatial resolution is 128 $\times$ 128 pixels.

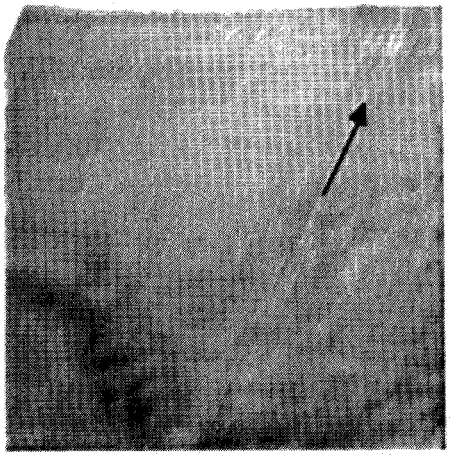

Fig. 3. A room-temperature image of a laser-ablated YBCO 1 in $\times$ 1 in film on a MgO substrate with the resolution of 256 $\times$ 256 pixels. The arrow shows direction of the X-scan (parallel to the narrow side of the slit). In contrast to Fig. 2, the dark regions here correspond to lower reflectivity.

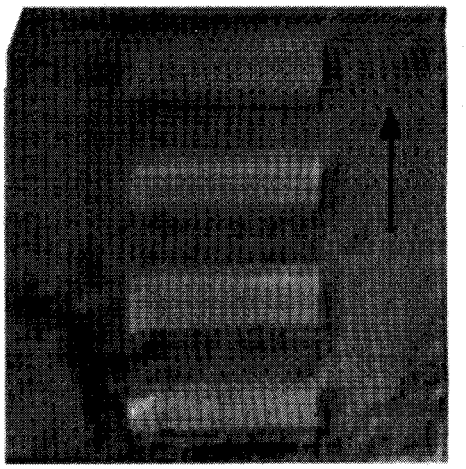

Fig. 4. A room-temperature image of the same YBCO film after vacuum deposition of silver through a mask. Note four silver rectangles in the center of the film.

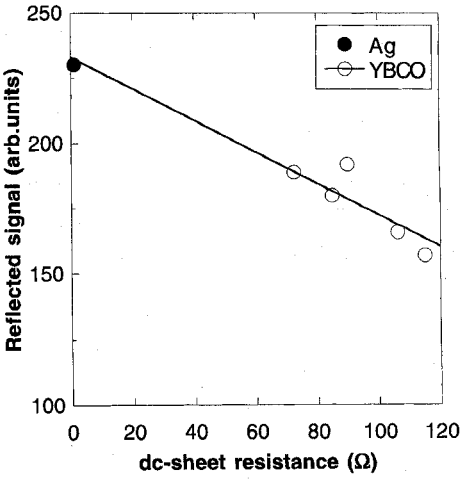

Fig. 5. Millimeter-wave reflectivity measured by the resonant slit probe versus dc sheet resistance for the YBCO film shown at the Fig. 3 (see text). The straight line shows a linear approximation that is only a guide to the eye.

and may be as small as $\lambda/100$. The ultimate resolution is determined by the minimal width of the slit, but it cannot be smaller than the skin-depth in the material from which the slit is fabricated, i.e., 1 μm (since the skin-depth in copper is 0.3 μm at 100 GHz). The spatial resolution in the direction parallel to the slit is determined by the field pattern in the slit and by the slit's length a', so that for the flat slit it is $\sim\lambda/2$. The resolution in this direction may be considerably improved (down to $\lambda/60$) if the slit is fabricated in the curved surface. This improvement originates from the strong decay of the field upon increasing distance from the slit, so that the central part of the slit (which is most close to the tested surface) plays a dominant role. Additional field concentration may be achieved using a dielectrically filled waveguide. The resulting spatial resolutions of the resonant slit probe in two perpendicular directions are still different, i.e., this probe has a considerable astigmatism. However, by doing scans in several directions and using deconvolution techniques and image processing, it is possible to achieve two-dimensional (2-D) resistivity maps with equal resolution in all directions.

III. Experimental

Fig. 1 is a schematic of our device. It operates in the reflection mode and consists of an HP 83558A millimeter-wave source and an E-band bridge based on a hybrid tee. The bridge is terminated by a sensing probe. The probe is matched by the E-H tuner in such a way that in the absence of the sample there is no reflection. The sample is mounted in the near-field of the probe, so that the sample-probe separation is $\sim$10–100 μm. The bridge goes out of balance due to reflection from the sample. The imbalance signal is measured by the Hughes 44 804H crystal detector and SR830-DSP lock-in amplifier. The raster scanning of the sample under the probe yields reflectivity map. In order to do phase measurements, the attenuator in the reference arm is set to a certain attenuation (so that the detector is always in the square-law regime) and the scanning is done twice for two settings of the phase shifter, differing by 180°. The recorded data are processed by MATLAB in order to calculate the amplitude and phase. Then a 2-D image of the reflectivity is generated using MATLAB and Adobe Photoshop software. The XY-translation stage with the resolution of 0.02 μm and the travel of 2 in $\times$ 2 in is used for the sample positioning. The mapping of an 1 in $\times$ 1 in film with the spatial resolution of 128 $\times$ 128 pixels takes an hour.

The sensing tip was prepared as follows. First, we fabricate a dielectric insert (made from teflon or high-density polyethylene) with a convex or wedge-like tip protruding from the waveguide. Then, this insert is covered by a 2- μm-thick silver coating, using vacuum deposition through a mask formed by a 20- μm-thick gold wire. The Q-factor of such a slit is 400–500. The whole geometry of our

probe reminds a magnetic head in the tape-recorder with one clear distinction. While the magnetic head has a cylindrical surface with a narrow slit cut *parallel* to the curvature axis, our millimeter-wave probe has a cylindrical surface with a narrow slit cut *perpendicular* to the curvature axis.

Fig. 2 demonstrates an amplitude image of a part of the NIST resolution target (Cr coating on glass, linewidth is 63 μm). Dark regions correspond to metal coating. We observe that the spatial resolution is of the order of $\lambda/60$ in both directions, and it is determined by the slit's width ($b' \approx 50$ μm) rather than by the wavelength ($\lambda = 3.8$ mm).

We have studied five laser-ablated YBCO films from different sources (Synergy, Fuba, ESPCI). Thick and optically uniform 1 cm^2 films show almost uniform millimeter-wave images. Fig. 3 demonstrates an image of a 1 in $\times$ 1 in film, which is not of high quality. Visual inspection of this film reveals decreased film thickness in one of the corners. A millimeter-wave image (Fig. 3) of the same film reveals an arc-like defect in the same corner. Since the film thickness (0.3 μm in average, as stated by the manufacturer) is small compared to the skin-depth ($\sim$10 μm), the contrast in the Fig. 3 must arise from the variation of the microwave *sheet resistance*. Fig. 4 demonstrates an image of the same YBCO film with four vacuum-deposited 1 μm-thick silver rectangles. In this case the contrast arises from the variation of *surface impedance*, since the thickness of the silver coating is bigger than the skin-depth (≈ 0.3 μm).

The millimeter-wave reflectivity image (Figs. 3 and 4) corresponds to the resistivity map as the reflection coefficient of a plane electromagnetic wave from conducting surface is directly related to the conductivity σ according to

$$\Gamma = \left(\frac{Z_0 - Z_s}{Z_0 + Z_s}\right)^2 \tag{3}$$

where $Z_s = (i\omega\mu_0/(\sigma + i\omega\varepsilon))^{1/2}$ is the surface impedance and ε is the dielectric constant. Following Tabib-Azar *et al.* [10], we assume that similar expression holds for the reflectivity in the near-field zone. Of course, in order to unambiguously yield resistivity using our technique, it is necessary to know the distribution of the near-field of the resonant slit. We are not aware of any calculations or simulations of the near-field of the resonant slit aperture in the presence of conducting surface. Therefore, we studied this question experimentally by comparing reflectivity from the areas with different dc-resistivities. In such an experiment it is very important to maintain a constant separation between the sample and the probe. Since our largest film turned out to be nonuniform (Fig. 3) we used different regions of this film as different sampling zones. We cleaned the film and deposited six silver stripes (not shown here) stretching from one side of the film to another, so that the film is divided into five separate regions. Then we measured dc-sheet resistance of each region, using these silver stripes as contacts. Afterwards, we marked the same regions in the millimeter-wave reflectivity map (Fig. 3) and calculated average reflectivity for each region. Fig. 5 demonstrates averaged millimeter-wave reflectivity vs sheet resistance. A clear correlation is observed. Reflectivity decreases with increasing sheet resistance.

By using our technique in the reflection mode, we map the normal-state *sheet resistance* of thin high-T_c films. The sheet resistance is $R = \rho/d$ where ρ is the film resistivity and d is the film thickness. By operating our technique also in the transmission mode, it would be possible to determine thickness and resistivity separately and to produce a resistivity map. Since the normal-state resistivity correlates with the superconducting properties [14], the *resistivity* map will bear an important information about uniformity of superconducting properties. The extension of our mapping technique to the measurements in the superconducting state are underway.

While the spatial resolution of our device is comparable to that of existing near-field microwave techniques, it has certain advantages.

1) The resonant slit has a much higher transmission coefficient than the small circular aperture [6]. This permits either a faster acquisition rate or better spatial resolution due to possibility of constructing smaller tips while maintaining the same signal-to-noise ratio.
2) In comparison to the miniature coaxial probe [7], [8] the resonant slit is easier to fabricate, since it is made by usual lithography.
3) In comparison to the microstripline resonator probe [10], the resonant slit is capable of operation in the pulse regime.
4) Operation of our device is distinctly different from that of the SQUID imaging [11] in two aspects: i) it does not necessarily require probe *cooling* and ii) it produces *coherent* images (i.e., amplitude and phase are mapped simultaneously).

ACKNOWLEDGMENT

The authors greatly appreciate the suggestions and discussions with M. R. Beasley and A. Frenkel. They are grateful to S. Chokron of Synergy, Jerusalem, to J. P. Contour, ESPCI, Paris, and to A. Jacobs of TU Braunschweig for YBCO films.

REFERENCES

[1] R. Wiesendanger, *Scanning Probe Microscopy and Spectroscopy.* U.K.: Cambridge Univ. Press, 1994.
[2] R. Gerber, D. Quenter, T. Doderer, C. A. Kruelle, R. P. Huebener, F. Muller, J. Niemeyer, R. Popel, and T. Weimann, "Quantitative measurement of the microwave distribution in superconducting tunnel junctions," *Appl. Phys. Lett*, vol. 66, pp. 1554–1556, 1995.
[3] J. J. Kopanski, J. R. Lowney, D. S. Miles, D. B. Novotny, and G. P. Carver, "High spatial resolution mapping of resistivity variations in semiconductors," *Solid-State Electronics*, vol. 35, pp. 423–433, 1992.
[4] J. S. Martens, V. M. Hietala, D. S. Ginley, T. E. Zipperian, and G. K. G. Hohenwarter, "Confocal resonators for measuring the surface resistance of high-temperature superconducting films," *Appl. Phys. Lett.*, vol. 58, pp. 2543–2545, 1991.
[5] A. T. Fiory, A. F. Hebard, P. M. Mankiewich, and R. E. Howard, "Penetration depths of high-T_c films measured by two coil mutual inductance," *Appl. Phys. Lett.*, vol. 52, pp. 2165–2167, 1988.
[6] E. A. Ash, G. Nicholls, "Super-resolution aperture scanning microscope," *Nature*, vol. 237, pp. 510–512, 1972.
[7] C. A. Bryant and J. B. Gunn, "Noncontact technique for the local measurement of semiconductor resistivity," *Rev. Sci. Instr.*, vol. 36, pp 1614–1617, 1965.
[8] R. Merz, F. Keilmann, R. J. Haug and K. Ploog, "Nonequilibrium edge-state transport resolved by far-infrared microscopy," *Phys. Rev. Lett.*, vol. 70, pp. 651–653, 1993.
[9] E. J. Spada, V. R. Rao, I. Bhat, and J. M. Borrego, "Non-destructive characterization of HgCdTe using photoinduced microwave refelection," *Semicond. Sci. Technol.*, vol. 8, pp. 937–940, 1993.
[10] M. Tabib-Azar, N. S. Shoemaker, and S. Harris, "Nondestructive characterization of materials by evanescent microwaves," *Meas. Sci. Technol.*, vol. 4, pp. 583–590, 1993.
[11] R. C. Black, F. C. Wellstood, E. Dantsker, A. H. Miklich, D. T. Nemeth, D. Koelle, F. Ludwig, and J. Clarke, "Microwave microscopy using a superconducting quantum interference device," *Appl. Phys. Lett.*, vol. 66, pp. 99–101, 1995.
[12] T. Moreno, *Microwave Transmission Design Data.* Dover, 1958, p. 154.
[13] V. F. Veley, *Modern Microwave Technology.* Englewood Cliffs, NJ: Prentice Hall, 1987, p. 157.
[14] A. Andreone, A. Cassinese, M. Iavarone, R. Vaglio, I. I. Kulik, and V. Palmieri, "Relation between normal-sate and superconductive properties of niobium sputtered films," *Phys. Rev. B.*, in press.